

Gold Nanoparticles Loaded with Chitosan Encapsulate Donepezil as a Novel Nanocomposite for Alzheimer's Disease Therapy

Lina Mohammad Saleh Al-Sarayra^a, Samer Hasan Hussein-Al-Ali^{a,b,*} , Mike Kh. Haddad^c ,
Abed Abdel Qader^b 

^aIsra University, Faculty of Pharmacy, 11622, Amman, Jordan.

^bIsra University, Faculty of Sciences, 11622, Amman, Jordan.

^cIsra University, Faculty of Engineering, 11622, Amman, Jordan.

Received: August 16, 2023; Revised: December 11, 2023; Accepted: December 28, 2023

Alzheimer's disease (AD) is the most common cause of dementia worldwide. Fifty million people today are affected by this disease globally. AD has had a tremendous impact on the affected individual, caregiver, and society, in both developed and developing nations. Donepezil—chitosan-gold nanocomposite (Donz-CS-AuNPs) was prepared by co-precipitation technique. Plackett-Burman experimental design was used in this work to estimate the effect of the three independent variables (concentration of chitosan, gold, and donepezil) on the dependent variables (loading efficiency, and particle size) by using Minitab 18.1 software. The quantities for the independent variables used were: 10 and 40 mg of donepezil, 24.6 and 73.8 mg of gold, and 500 and 1500 mg of chitosan. The Donz-CS-AuNPs were characterized using energy dispersive X-ray (EDX) analysis, X-ray diffraction (XRD), scanning electron microscopy (SEM), Fourier transform infrared spectroscopy (FTIR), UV-Vis spectroscopy and release study. The results of EDX showed strong signals of Au (1.5–2, 2–2.5 and 9.5–10 keV), which confirmed the specific gold peaks from the Donz-CS-AuNPs. The XRD pattern of Donz-CS-AuNPs nanocomposites showed the existence of AuNPs peak at $2\theta = 38.2^\circ$, 43.8° and 64.5° . The SEM images demonstrated spherical shapes of the AuNPs. In the *in vitro* release study, the release increased steeply and reached 75% after 1440 min.

Keywords: Gold nanoparticles, Alzheimer's disease, Donepezil, Controlled release.

1. Introduction

A drug delivery system is a formulation or device that allows a drug and other substances to be introduced into the body and increases its safety and efficacy by managing the time, rate, and location of drug release in the body. A drug delivery includes the administration of the therapeutic product, the release of the active substance by the product, and the transport of the active ingredients across biological membranes to the site of action¹.

Nanoparticles (NPs) are microscopic particles with dimensions less than 100 nm and have numerous applications. NPs are constantly being developed in medicine for medication delivery, disease screening, and tissue engineering². NPs can be classified into several groups, such as polymeric NPs, dendrimers, micelles, liposomes, and inorganic NPs like gold NPs, quantum dots, and super magnetic iron oxide³⁻⁷.

The exceptional properties of NPs, such as higher therapeutic efficacy, higher stability, lower toxicity, ability to encapsulate, and the ability to deliver both hydrophilic and hydrophobic drugs and change undesirable pharmacokinetics of drugs, enable them to be used in medicine as therapeutics carriers and for diagnostic purposes³.

Two methods are used for the preparation of gold NPs (AuNPs): 'top-down' and 'bottom-up'. The 'top-down'

method requires more energy and instrumentation and causes defects in the surface structure of the products, which impact their physicochemical properties⁸⁻¹⁰. The 'bottom-up' method involves the self-assembly of gold atoms into uniformly sized AuNPs, which is easily controlled and cost-effective¹¹. The bottom-up method has different preparation ways, including biosynthesis, chemical synthesis (chemical reduction, spinning, and sol-gel process), and physical methods (photochemical, electrochemical, and sonochemical)^{12,13}. The chemical reduction method for AuNPs has different merits because of its homogeneity, dispersion, enhanced stability, and precise control over size and shape.

AuNPs have many properties, such as surface plasmon resonance (SPR), and because of their surface's capacity to be functionalized with a wide range of ligands, they are actively involved in drug delivery, diagnostics, therapy, and bio-sensing¹⁴.

Donepezil (Donz) is a centrally acting, reversible and noncompetitive acetyl cholinesterase (AChE) inhibitor used to inhibit AChE, which causes degradation of ACh in nucleus basalis and associated areas and hence increases the concentration of ACh in the brain, and enhances cholinergic neurotransmission¹⁵. Donz is used to treat Alzheimer's disease in people who have mild to moderate symptoms. It is metabolized into four primary metabolites by the CYP

*e-mail: samer.alali@iu.edu.jo

450 isoenzymes 3A4 and 2D6, followed by glucuronidation and urine elimination. To obtain better bioavailability, smaller pharmacological molecules with low aqueous solubility (0.0045 mg/mL) must be synthesized either using a micellar method or maybe employing NPs¹⁶.

Many researchers used Donz-NPs to increase the delivery of the drug to the brain via the olfactory pathway and across the blood-brain barrier (BBB), such as Donz-PLGA-b-PEG polymer or Donz-chitosan¹⁷.

Chitosan is a natural biodegradable and linear polysaccharide consisting of β -(1 \rightarrow 4)-linked D-glucosamine (deacetylated unit) and N-acetyl-D-glucosamine (acetylated unit) that are randomly distributed. The majority of chitosan is positively charged in an acidic environment, as a result of the presence of amino groups¹⁸.

Chitosan (CS) is broadly used in drug delivery systems as a carrier and is considered very effective as a reducing agent and stabilizing agent for preparations of AuNPs¹⁹. Additionally, CS as a cationic polymer gives a positive charge to the surface of AuNPs and enhances their affinity to negatively charged targets such as nucleic acids and cell membranes^{20,21}. A double electric layer around the AuNPs is generated by an ionic surfactant possessing extended end chains, and a CS polar head group which offers steric repulsion within the AuNPs, thus preventing the agglomeration of AuNPs, and giving rise to a mutual stabilization system^{22,23}.

In recent years, the interest in neurodegenerative illnesses has increased. Different methods are being studied to increase drug uptake in the brain by crossing the BBB, which isolates and protects the brain from the entry of unwanted molecules circulating in the blood. The BBB is characterized by having impermeable endothelial cells with tight junctions, an active efflux transport system and enzymatic activity, which permit specific and selective molecules to enter the brain, which consequently means that many useful drugs are excluded²⁴. Therefore, drugs which have problem in stability, solubility, selectivity, toxicity, and multiple doses can be resolved by using suitable NPs.

Despite the obvious usage of NPs to increase drug delivery in the brain via multiple methods of administration, 2-5 particles larger than 250–300 nm are an ineffective drug delivery in the brain due to lower penetration transport across paracellular and intracellular areas. These limitations can be solved by using nanocarriers, which result in effective medication transport across the BBB.

The aim of the current study is to prepare and characterize CS-encapsulated Donz with subsequent loading on AuNPs to generate a novel ternary system of Donz-CS-AuNPs nanocomposites for the first time. Plackett-Burman experimental design was used in this work to estimate the effect of the three independent variables (concentration of chitosan, gold, and donepezil) on the dependent variables (loading efficiency, and particle size).

2. Materials and Methods

2.1. Materials

Gold chloride trihydrate ($\text{HAuCl}_4 \cdot 3\text{H}_2\text{O}$) with molecular weight 393.83 g/mol, chitosan polymer with low molecular weight, and donepezil ($\text{C}_{24}\text{H}_{29}\text{NO}_3$) with molecular weight

415.95 g/mol used in this study were purchased from Sigma Aldrich Company (USA). Sodium borohydride (NaBH_4) with molecular weight 37.83 g/mol, was purchased from Oxford company (India). Phosphate buffer saline solution with a composition of 0.0027 M potassium chloride and 0.137 M sodium chloride, pH 7.4, was purchased from Sigma-Aldrich (United States).

2.2. Design of experiment

Plackett-Burman experimental design was used in this work to estimate the effect of the three independent variables (concentration of chitosan, gold, and donepezil) on the dependent variables (percent loading efficiency, and particle size) by using Minitab 18.1 software. The levels for the independent variable's levels were obtained by Plackett-Burman design and were as follows: Donz (10 and 40 mg), gold (24.6 and 73.8 mg) and CS (500 and 1500 mg).

2.3. Preparation of CS-AuNPs

The sodium borohydride was prepared by dissolving 29.8 mg in 40 ml distilled water. Gold chloride trihydrate solutions were prepared by dissolving 24.6 and 73.8 mg into 50 ml distilled water. In addition, the chitosan solution was prepared by dissolving 0.5 and 1.5 mg of chitosan in 2% acetic acid.

The CS-AuNPs were prepared by mixing the solution of chitosan with gold. After that, sodium borohydride was added to the mixture of solutions, and the colloid formed was an intense red color. The AuNPs formed were constantly stirred for one hour, then centrifuged for one hour at a speed of 11000 rpm, then washed in distilled water, and finally dried in the oven at 40 °C.

2.4. Preparation of Donz-CS-AuNPs nanocomposites

To prepare the Donz-CS-AuNPs nanocomposites, 10 and 40 mg of Donz were dissolved in distilled water and mixed with a solution of gold and chitosan. Sodium borohydride solution was then added to the last mixture of solutions. The solution color changed to red, which indicates formation of Donz-AuNPs. The components were stirred for one hour, then centrifuged for 1 hour at a speed of 11000 rpm, then washed in distilled water, and finally dried in the oven at 40 °C.

2.5. Determination of the loading efficiency of Donz in Donz-CS-AuNPs nanocomposites

The loading efficiency of Donz in the nanocomposites was calculated using ultracentrifugation equipment and the following equation:

$$\% \text{Loading Efficiency} = \frac{\text{Concentration of drug used} - \text{Concentration of drug in supernatant}}{\text{mass of nanocomposite}} \times 100$$

2.6. In vitro release study of Donz from Donz-CS-AuNPs nanocomposites

Perkin Elmer UV-vis spectrophotometer was used to estimate *in vitro* release of Donz from the nanocomposites in a potassium buffer phosphate (PBS) at pH 7.4. Suitable

amounts of each nanocomposite were mixed with PBS. The total amount of Donz released into the release media was automatically measured every 10 minutes for the next 24 hours at the corresponding λ_{\max} . Percent release of Donz in the PBS was calculated as per the below equation:

$$\% \text{Release} = \frac{\text{Concentration of drug at time } t \text{ (ppm)}}{\text{Concentration of drug in the nanocomposites (ppm)}} \times 100$$

2.7. Optimization of the best model

Response surface methodology (RSM) is a one statistical and mathematical tool used to optimize the influences of process variables based on the design of an experiment. RSM minimizes the number of trials and indicates how process parameters influence the removal process. In the present study, optimal conditions were obtained at the highest loading efficiency, and the lowest particle size.

2.8. Instrumentation

Powder X-ray diffraction (XRD) patterns were used to determine the crystal structures of the AuNPs and Donz-CS-AuNPs nanocomposites samples over a range of 30° – 85° , using an XRD-6000 diffractometer (Shimadzu, Tokyo, Japan) with $\text{CuK}\alpha$ radiation (λ 1.5406 Å) at 30 kV and 30 mA. Fourier transform infrared (FTIR) spectra of the materials were recorded over a range of 400 – $4,000$ cm^{-1} using a Perkin Elmer (model smart UAIR-tow). ANOVA™ Nano SEM 230 (FEI, Hillsboro, OR USA) scanning electron microscope (SEM) was used to observe the surface morphologies of the samples. Ultraviolet-visible spectra were generated both to determine the optical properties and for controlled release studies, using an ultraviolet-visible spectrophotometer (PerkinElmer).

3. Result and Discussion

Minitab 18.1 software analyzed the results and determined the optimized formulation of Donz-CS-AuNPs. The design matrix is based on three factors: A, B, and C, representing concentrations of CS, Donz, and gold at varying levels of each factor, using the Plackett-Burman design (PBD).

The results were obtained for 12 experimental runs required for regression analysis. In Table 1 all factors (A,

B, and C) have been evaluated to illustrate the impact of factors on loading efficiency, and particle size.

3.1. Effect of formulation factors on loading efficiency (LE%) and particle size

3.1.1. Analysis of variance (ANOVA) for loading efficiency (LE%)

ANOVA is a structural system that serves as the basis for significance tests and gives information about the levels of variability within a regression model and can be used to detect the reliability of a design model by reducing random variability. In ANOVA analysis, the p-value is a statistical measurement used to test a hypothesis against actual data to decide whether to accept or reject a null hypothesis. If the p-value is equal to 0.05 or lower, the system considers it statistically significant. There is an inverse relationship between p-values and F-values. Table 2 below demonstrates that the model is significant because the p-value is lower than 0.05 and the F-value is high. The two factors (CS and drug) have a significant effect on loading efficiency. This is because F-values are high and p-values are lower than (0.05) when compared with another factor (gold), which has a non-significant effect on loading efficiency because the p-value in this case is (0.076), which is higher than (0.05), and the F-value is low.

The CS concentration was shown to be a significant parameter for optimizing the loading efficiency of Donz-CS-AuNPs nanocomposites over a long time because of its dual activity; first, it acts as a stabilizing agent due to its high molecular weight and high viscosity, which prevents aggregation, and second, it acts as a reducing agent for the nanoparticles²⁵.

In addition, the drug concentration is also an essential parameter of the loading efficiency of the Donz-CS-AuNPs. As is evident in Table 3, an increase in loading efficiency occurred when the concentration of the drug increased, as a result of an increase in the chance of the drug particles binding with the AuNPs.

Lack of fit is a test used when data contains replicates (multiple observations with the same X-value). The p-value is compared to a significant level to determine whether the model accurately fits the data or not. If the p-value is equal

Table 1. Data results for loading efficiency (LE%), and particle size.

Run Order	CS (g)	Drug (mg)	Gold (mg)	%LE	Size (nm)
1	0.5	10.0	73.8	25.0	*
2	0.5	10.0	24.6	28.2	60
3	1.5	10.0	73.8	11.5	59
4	1.5	40.0	24.6	41.1	110
5	1.5	40.0	24.6	40.5	100
6	1.5	10.0	24.6	*	82
7	0.5	10.0	24.6	26.9	60
8	0.5	40.0	73.8	83.9	60
9	0.5	40.0	24.6	53.1	70
10	0.5	40.0	73.8	65.0	48
11	1.5	40.0	73.8	69.2	80
12	1.5	10.0	73.8	10.5	59

Table 2. Analysis of variance (ANOVA) for loading efficiency (LE%), and particle size.

Source	loading efficiency (LE%)							particle size						
	Adj SS	Adj MS	F Value	P Value	Coef	T Value	VIF	Adj SS	Adj MS	F Value	P Value	Coef	T Value	VIF
Regression	5141.9	1713.97	18.92	0.001				3545.21	1181.74	42.35	0.000			
CS	845.7	845.70	9.33	0.018	-17.81	-3.06	1.02	1849.19	1849.19	66.27	0.000	26.33	8.14	1.02
Drug	4565.0	4565.04	50.39	0.000	1.379	7.10	1.02	962.67	962.67	34.50	0.001	0.633	5.87	1.02
Gold	393.1	393.12	4.34	0.076	0.247	2.08	1.02	1493.63	1493.63	53.53	0.000	0.4810	7.32	1.02
Error	634.2	90.60						195.33	27.90					
Lack-of-Fit	454.0	151.35	3.36	0.136				73.33	24.44	0.80	0.554			
Pure Error	180.1	45.03						122.00	30.50					
Total	5776.1							3740.55						
R ²	R ² = 89.02%, R ² (adj) = 84.32%, R ² (pred) = 73.52%							R ² = 94.78%, R ² (adj) = 92.54%, R ² (pred) = 87.04%						
Regression equation	%LE = 9.30 - 17.81 CS + 1.379 Drug + 0.247 Gold							Particle size = 50.00 + 26.33 CS + 0.633 Drug - 0.4810 Gold						

VIF = variance inflation factor, *Adj SS = adjusted sums of squares, *Adj MS = adjusted mean squares, DF = degree of freedom

Table 3. Summary of validation parameters for loading efficiency (LE%), and particle size models.

Concentrations	Experimental response	Predicted values	Observed values	Bias (%)
Drug (10.0 mg)	LE (%)	32.4	35.5	9.6
CS-Polymer (0.5 g) Gold (73.8 mg)	Particle Size (nm)	34.0	39.2	15.3
Drug (20.0 mg)	LE (%)	31.1	29.5	-5.1
CS-Polymer (1.0 g) Gold (50.2 mg)	Particle Size (nm)	65.0	70.2	8.0
Drug (30.0 mg)	LE (%)	30.2	34.0	12.6
CS-Polymer (1.5 g) Gold (25.0 mg)	Particle Size (nm)	97.0	90.0	-7.2
% Bias was calculated as (observed value - predicted value) / predicted value × 100				

to (0.05) or lower, the model does not accurately fit the data. To get a better model in the experimental design, the “lack of fit F-value” must be insignificant. In this model, the lack of fit is (0.136), which is higher than (0.05) and insignificant.

To evaluate the model performance, analysis of determinate the coefficients R-squared (R^2), predicted R-squared, and adjusted R squared were tabulated in Table 2.

R-squared (R^2) is a statistical measure that shows the proportion of variation explained by an independent variable or variables in a regression model for a dependent variable. The R-squared value indicates how much the variation of one variable explains the variance of the other. The data of the model are fitted better when R^2 is high. R-squared is defined as the percentage ranging from (0 to 100), with 100 indicating perfect correlation and zero indicating no association. R-squared always increases as the number of effects is included in the model²⁶.

Adjusted R-squared is a variant of R-squared that considers the number of predictors in the model. When the effect improves the model more than expected by chance, the adjusted R-squared increases; when a predictor improves the model by less than expected, the value decreases. The adjusted R-squared is usually positive rather than negative. It is never greater than R-squared; it is less than or equal to R^2 ²⁷.

On the other hand, predicted R-squared measures how well a regression model predicts responses to new observations. This statistic indicates when the model fits the original data but is less capable of making valid predictions for new observations²⁸.

Table 3 calculates the ratio of total variability represented by the model. For loading efficiency, R-squared is 89.02% which is close to 100%, and indicates the model was reliable and closely fit actual data. As a result, the adjusted R-squared is 84.32%. R-squared is calculated to be 73.52% based on the prediction statistic. The difference between “predicted R^2 ” (73.52%) and “adjusted R^2 ” (84.32%) is 10.8%. This indicated that the “predicted R^2 ” is in a reasonable agreement with “adjusted R^2 ”. If there is a difference greater than 20%, a data problem or model distribution will occur²⁹.

In a multiple regression model, multicollinearity (variance inflation factor) occurs when high intercorrelations exist between two or more independent variables. When a researcher or analyst tries to figure out how well each independent variable can be utilized to predict or comprehend the dependent variable in a statistical model, multicollinearity can lead to skewed or misleading conclusions, as shown in Table 3. If the variance inflation factor (VIF) is more than 10, the factors in the regression are strongly associated, the regression coefficient has a high variance, the model is less reliable, and vice versa. Because the VIF values in Table 2 are (1.02), which is less than 10, the model has low variance on the regression coefficient and consequently low multicollinearity.

Adjusted sums of squares (Adj SS) are measurements of variation for various model components. The model's predictors' order does not affect the adjusted sum of squares calculation.

3.1.2. Analysis of variance (ANOVA) for particle size

Analysis of variance related to size is shown in Table 3. Using p-value models in the analysis showed that the chitosan, drug, and gold nanoparticles are statistically significant because of a p-value below 0.05 and a high F-value. Also, the lack of fit is insignificant due to the p-value being higher than 0.05.

In Table 2, the model demonstrates the proportionate total variability, which R-squared explains. R-squared has a value of 94.78%. As a result, the adjusted R-squared is calculated to be 92.54%. R-squared is calculated to be 87.04% based on prediction statistics. The difference between “predicted R²” (87.04%) and “adjusted R²” (92.54%) is 5.5%. This indicated that the “predicted R²” is in a reasonable agreement with “adjusted R²”.

The multicollinearity (VIF) values are (1.02), as shown in Table 2, indicating the variance of the regression coefficient for the size of the nanoparticle is low so that we can say the model is going to be reliable.

The T-value indicates the magnitude of the difference compared to the variation in the sample data. T is simply the calculated difference presented in standard error units. The

larger the magnitude of T, the more evidence there is a statistically significant difference. The closer T is to 0, the less likely a significant difference exists. In Table 2, the CS and drug are more statistically significant differences than gold nanoparticles.

3.2. Contour and surface plot contour and surface plot for loading efficiency and particle size

3.2.1. Contour plot and surface plot for loading efficiency

Contour plots are graphics used to visualize the relationship between loading efficiency and two continuous variables. In a contour plot, points with the same response value are joined to form contour lines in a two-dimensional (2D) view X-axis and Y-axis. In Figure 1(a-1), the region of highest loading efficiency appeared when using a high concentration of drugs and a wide range concentration of gold nanoparticles (50-70) mg. The effect of CS and gold nanoparticles on the loading efficiency is represented in Figure 1(b-1). This

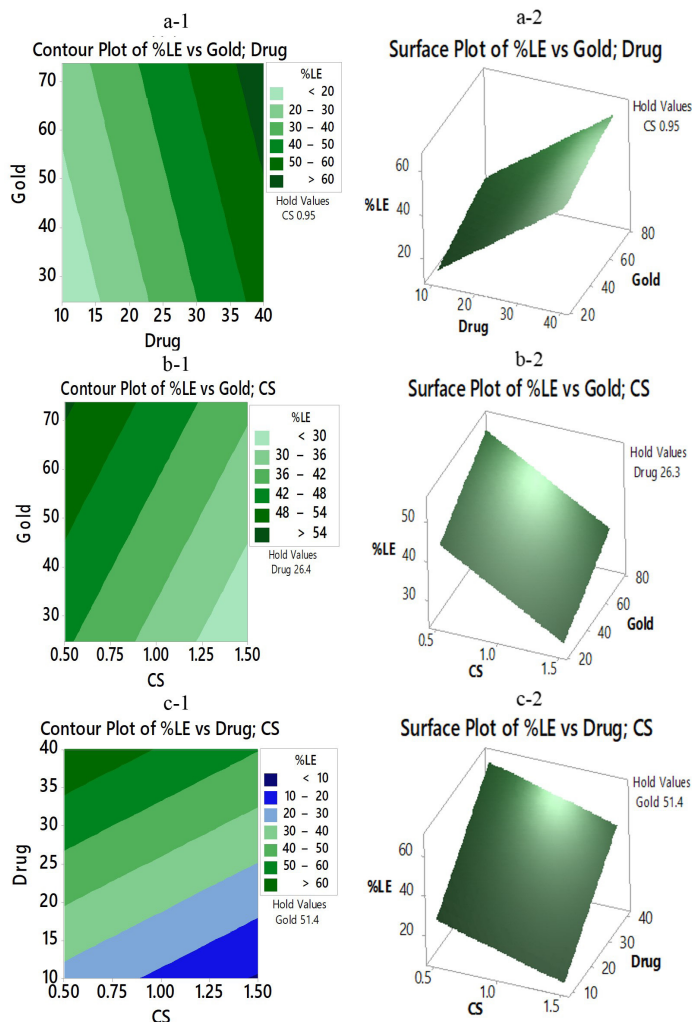


Figure 1. Contour plot and surface plot for loading efficiency against gold, drug, CS.

result reveals that the highest loading efficiency above 54% was obtained when the concentration of CS was very low and the concentration of gold very high. The last contour Figure 1(c-1) explains the relationship between CS and drug on the loading efficiency, and the results demonstrate that the highest loading efficiency was obtained when using a wide range of CS concentration (0.5-1) mg and a high concentration of the drug.

Surface plots are three-dimensional data representations. Surface plots illustrate a functional relationship between a set of dependent variables on the x- and y-axes and the response variable (loading efficiency) (z), which is represented by a smooth surface. Figure 1(a-2) represents the interaction plots between gold and drug with respect to loading efficiency (LE%); the response increases when the surface becomes darker. Therefore, the highest loading efficiency can be achieved by using a high concentration of drug and a wide range of AuNPs nanoparticles (50-70) mg.

Figure 1(b-2) shows the interaction plot between AuNPs and CS with respect to loading efficiency. The darker surface appeared when using a very small quantity of CS and a very high quantity of AuNPs to achieve loading efficiency equal to or above 54%.

Figure 1(c-2) illustrates the relationship between CS and drug on the loading efficiency, and the result showed that the highest loading efficiency can be achieved by using a high concentration of drug and a wide range of AuNPs (50-70) mg.

3.2.2. Contour plot and surface plot for particle size

The variables (gold, drug, and CS) that affect the particle size response are shown in Figure 2 as a contour plot and surface plot. Figure 2a-1 and Figure 2a-2 represent the interaction plot between gold and drug against particle size as output. The result illustrated in these figures is that the smallest particle size values can be obtained by decreasing the concentration of the drug and increasing the concentration of gold in the sample above 70 mg.

In Figure 2b-1, the contour plot showed that the smallest particle size was obtained at low concentrations of CS (0.5-0.7) mg and high concentrations of gold (62-70) mg; the surface is minimal in Figure 2b-2. In addition, Figures 2(c-1) and 2(c-2) show that the particle size is affected by using different concentrations of CS and drug. A small concentration of CS and drug is used to get a particle size less than 90 nm.

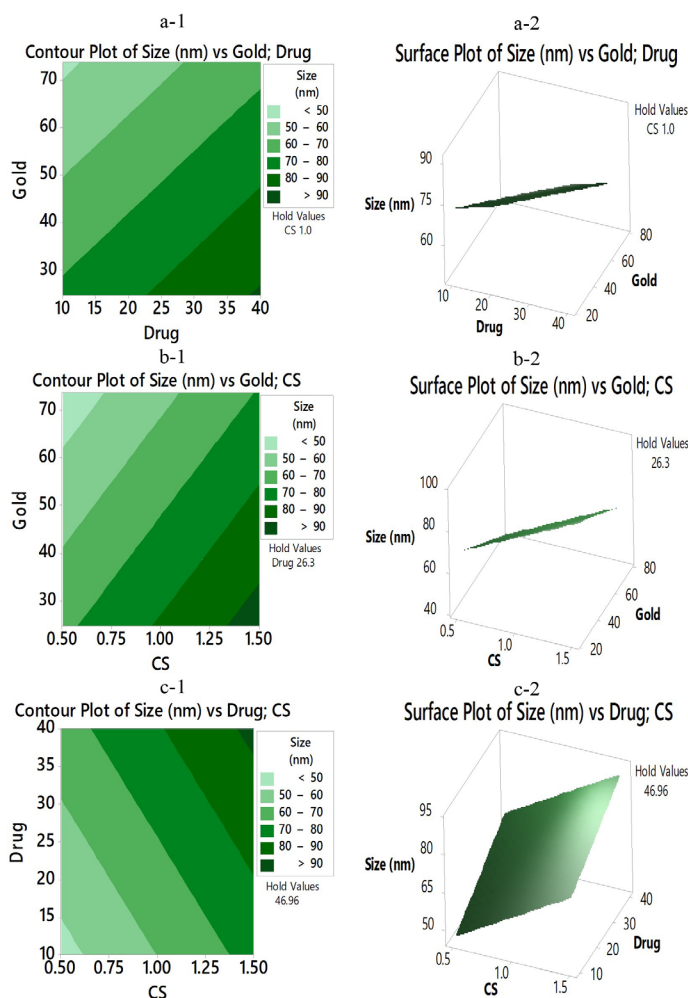


Figure 2. Contour and surface plots for particle size against gold, drug and CS.

3.3. Optimization of loading efficiency and particle size models

Response surface methodology (RSM) is a statistical tool used for optimization and finding the best set of factor levels to achieve a goal.

The main goal of RSM is to generate knowledge in the experimental domain of interest, accurately estimate experimental variability, propose sequential strategies for carrying out the experiment with various alternatives based on the results obtained, and make decision-making possible under uncertain conditions while reducing ambiguity.

To obtain an optimum formula with the highest loading efficiency and smallest particle size, (1.5) g of CS, (39.1975) mg of the drug, and (24.6) mg of gold is needed. This will produce a formula with (42.7183%) loading efficiency, and (102.4918) mg of particle size.

3.4. Validation of loading efficiency, and particle size models

The validation of a model is described as comparing the model's forecasts to the values observed in the existing system to determine if the model is valid for the intended purpose. To examine validation, the value of bias on the system is used. The bias of an estimator in statistics is the difference between the estimator's expected value and the

actual value of the parameter being evaluated. An unbiased estimator or decision rule has zero bias.

Table 3 demonstrates the percentage of bias between predicted and observed values to determine if the model is valid or not. In the first formula, when (drug = 10.0 mg), (CS-polymer = 0.5 g), and (Gold = 73.8 mg), the bias values were (9.6%, 15.3%) for LE (%) and particle size (nm), respectively. For the second formula, bias values were (-5.1%, 8.0%) for LE (%) and particle size (nm), respectively, when (drug = 20.0 mg), (CS-polymer = 1g), and (gold = 50.2 mg). Finally, the third formula had bias values of (12.6%, -7.2%) for LE (%), and particle size (nm), respectively, when the concentrations were (drug = 30.0 mg), (CS-polymer = 1.5 g), and (gold = 25.0 mg). The result demonstrated that the model is valid because there is a good correlation between predicted and experimental values.

3.5. Characterization of Donz-CS-AuNPs nanocomposites

3.5.1. EDX spectra of Donz-CS-AuNPs nanocomposites

Element composition of Donz-CS-AuNPs nanocomposites deposited on IDE thin films is shown in Figure 3a. In this study, respective relevant spectrums with strong signals of

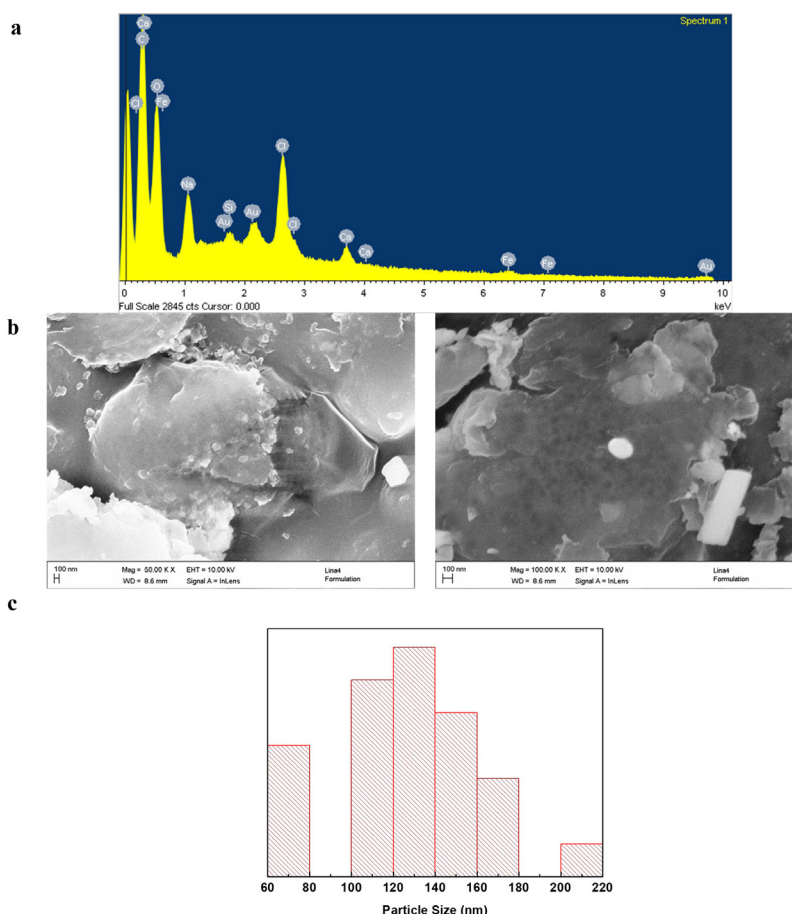


Figure 3. EDX spectrum of CS-AuNPs nanoparticles (a), scanning electron microscopes (b), and histogram for particle size distribution (c).

Au (1.5–2, 2–2.5 and 9.5–10 keV) at characteristic energy were observed, which confirmed the specific gold peaks from the sample. In addition, the oxygen, chlorine, and sodium were found in traces due to water moisture and carbon adhesive used in the sample preparation prior to taking the SEM micrograph for the EDX profile. Signals from iron and other elements originated from grid³⁰. As shown in Figure 3b, the SEM images demonstrated spherical shapes of the CS-AuNPs, and the average diameter was 130 nm (Figure 3c).

3.5.2. XRD analysis

XRD analysis was carried out to confirm and identify the crystalline structure of the Donz-CS-AuNPs nanocomposites containing CS. Figure 4 shows the representative XRD pattern of the Donz-CS-AuNPs nanocomposites prepared by chemical method after complete reduction of Au³⁺ to Au⁰. The XRD pattern of Donz-CS-AuNPs nanocomposites showed the existence of CS peak at $2\theta = 19.4^\circ$, as well as those of CS-AuNPs at $2\theta = 38.2^\circ$, 43.8° and 64.5° , which can be due to the 111, 200 and 220 planes, respectively. These three peaks confirmed that the CS-AuNPs exist in the face centered cubic crystal structure according to JCPDS card no. 04-0784³¹. From the literature, donepezil hydrochloride (Donz-HCl) represented a crystalline nature with three peaks at $2\theta = 6.64^\circ$, 6.87° , and 13.00° ³². In our work, the absence of Donz-HCl peaks confirmed that the drug was dispersed in the CS³².

3.5.3. FTIR analysis

The FT-IR scans of both Donz-HCl and the Donz-CS-AuNPs nanocomposites were scanned. The FT-IR of pure Donz-HCl revealed a sharp peak at 3586 cm^{-1} as seen in Figure 5a, which corresponds to the water of hydration. At 1683 cm^{-1} , the most intensive band indicated a stretching vibration of the C=O group in the structure. Another band from C=C in the aromatic ring appeared around 1601 cm^{-1} . However, the sharp absorption band of C-N in the structure appears at 1315 cm^{-1} .

The FTIR spectra of CS-AuNPs were analyzed from the literature to detect potential interactions between CS functional groups and AuNPs. Chemical interactions between two or more substances are represented as a shift or changes in the characteristic spectrum peaks. The FTIR spectra of CS-AuNPs showed nearly identical peaks to pure CS,

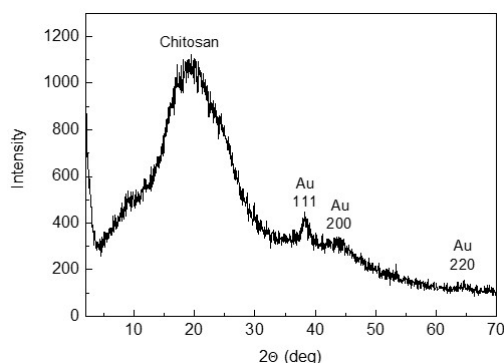


Figure 4. XRD patterns of the Donz-CS-AuNPs nanocomposites.

indicating uniform CS deposition over AuNPs. The main difference between CS-AuNPs and pure CS in the FTIR is the shifting in the broad band of (O–H or N–H) groups from ($3357\text{--}3271\text{ cm}^{-1}$) to ($2992\text{--}2901\text{ cm}^{-1}$), and the removal of a peak at 2856 cm^{-1} . Figure 5b demonstrates FTIR spectrum of Donz-CS-AuNPs nanocomposites.

The CS in this work acts both as a reducing and stabilizing agent, by reducing the Au⁺³ ions to Au (0), thus forming the AuNPs. According to literature, the electrostatic forces between the positively charged amino groups in CS and the negatively charged AuNPs, led to the preparation of CS-AuNPs with high stability^{33,34}. Figure 6 shows the expected interaction between Donz and CS-AuNPs.

3.5.4. UV – scan of CS-AuNPs

CS-AuNPs have a unique optical property known as localized surface plasmon resonance (LSPR), which is the collective oscillation of electrons in the conduction band of gold nanoparticles in resonance with a specific wavelength of incident light. Using UV-Vis spectroscopy, CS-AuNPs LSPR produces a high absorbance band in the visible region (517 nm) (Figure 7).

3.5.5. In vitro study of Donz release from the Donz-CS-AuNPs nanocomposites

In vitro, Donz release tests from Donz-CS-AuNPs nanocomposites were performed using phosphate-buffered saline (PBS) medium at pH 7.4 to simulate intestinal fluid. As seen in Figure 8, the first-time release (from 0-150 minutes) showed slow release. Then, the release

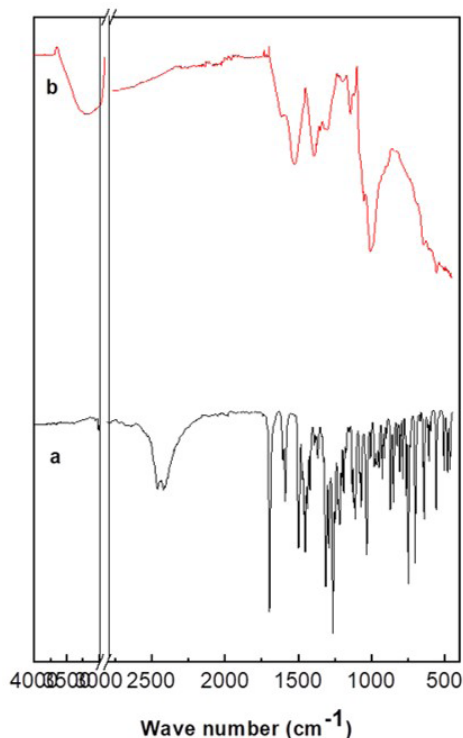


Figure 5. The FT-IR spectra of Donz-HCl (A), and Donz-CS-AuNPs nanocomposites (B).

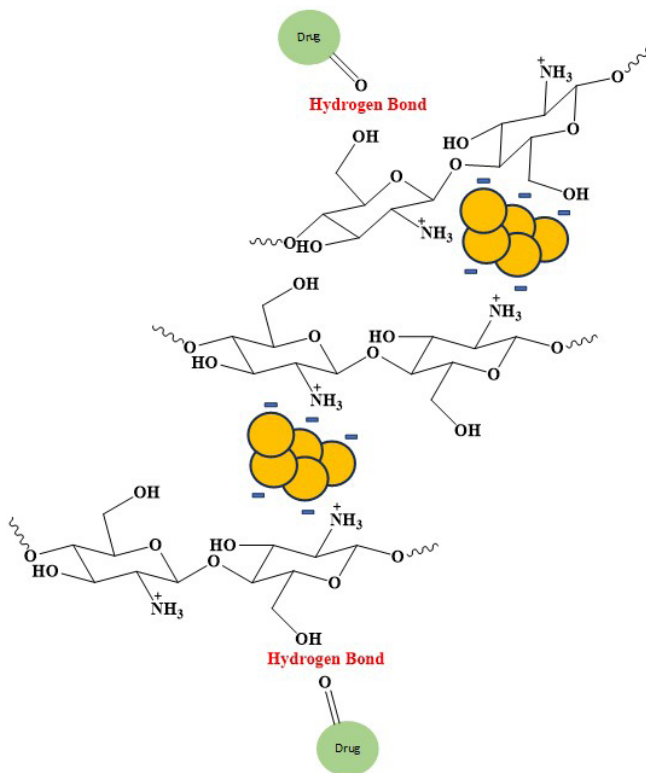


Figure 6. Interaction between Donz and CS-AuNPs.

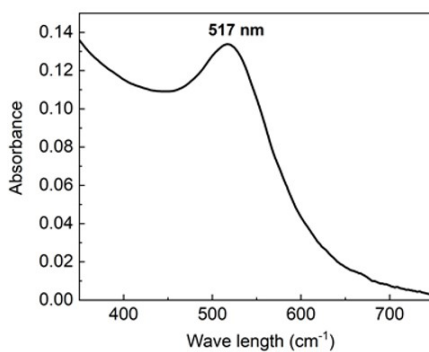


Figure 7. UV-Visible spectra of CS-AuNPs.

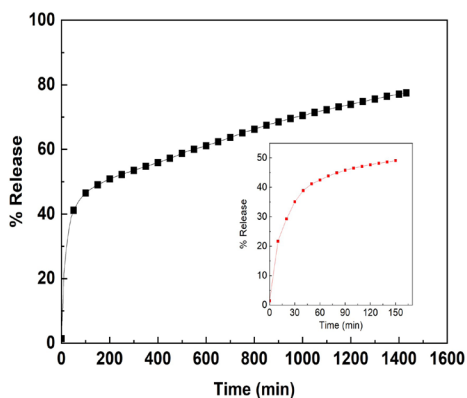


Figure 8. Release profiles of the Donz from Donez-CS-AuNPs at pH 7.4.

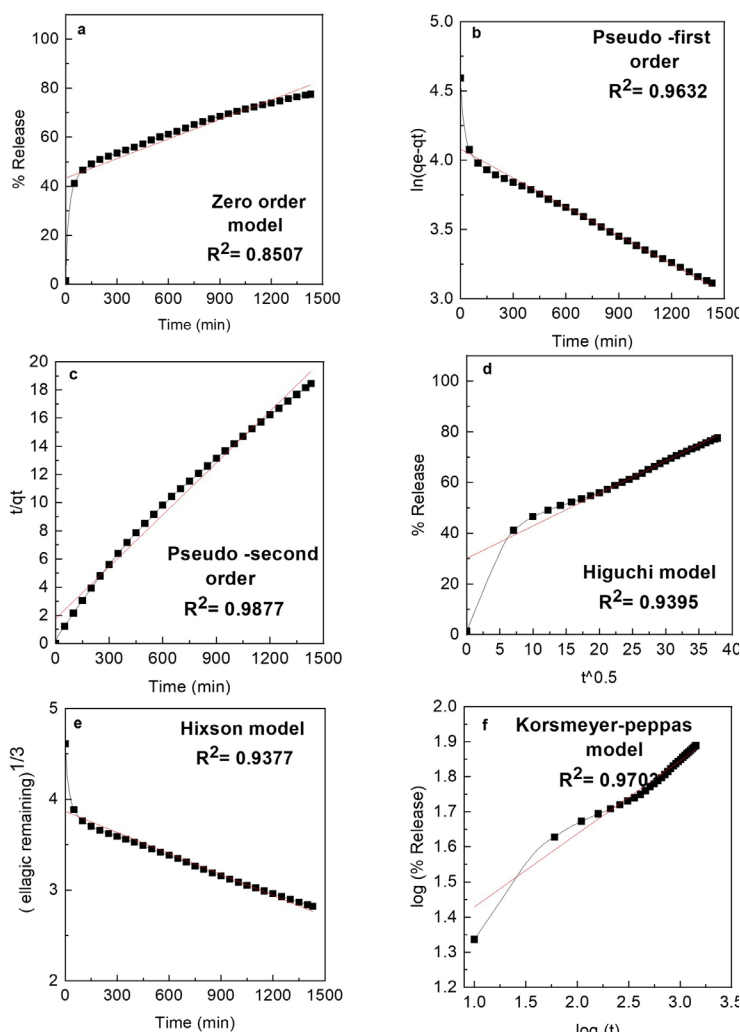


Figure 9. Data fitting for Donz release from Donz-CS-AuNPs nanocomposites using different kinetic models.

Table 4. The kinetics equations of the models used in fitting the Donz drug release data.

Models	Equation
Zero order	$q_t = k_0 t$
Pseudo-first order	$\ln(q_e - q_t) = \ln q_e - k_1 t$
Pseudo-second order	$t/q_t = 1/k_2 q_e^2 + t/q_e$
Higuchi	$q_t = K_H \sqrt{t}$
Hixson-Crowell	$\sqrt[3]{M_0 - q_t} - \sqrt[3]{q_t} = Kt$
Korsmeyer-Peppas	$\frac{q_t}{q_\infty} = Kt^n$

k_1 is the rate constant for each release kinetics. q_e is the quantity released at equilibrium. q_t is the quantity released at any time (t). M_0 is the initial quantity of drug in the nanocomposite. q_∞ is the release at infinite time.

from Donz-CS-AuNPs nanocomposites increases steeply with controlled release properties³⁵. The maximum release

reached 75% after 1440 min. These results were due to the ionic interactions between the Donz drug and CS-AuNPs.

3.5.6. Donz-CS-AuNPs release kinetics

The release behaviors of Donz from Donz-CS-AuNPs nanocomposites can be explained by the different kinetics models shown in Table 4³⁶.

Donz release kinetics from the Donz-CS-AuNPs nanocomposites is shown in Figure 9 with regression coefficient (R^2) values. The model that gave greater R^2 values was studied in a selected fit model. It was also seen that the release of Donz from Donz-CS-AuNPs nanocomposites followed the Pseudo-second order kinetic model^{37,38}.

4. Conclusion

In conclusion, the overall goal of this study has been achieved by preparing Donz-CS-AuNPs to enhance the delivery of the drug to the brain by using CS as a stabilizing agent, and sodium borohydride as a reducing agent of gold. The minitab18.01 software was used to determine the best

formulation of Donz-CS-AuNPs nanocomposites, and evaluate factors affecting loading efficiency, and particle size. The results revealed that loading efficiency is affected by the concentration of CS and drug so that the higher concentration of drug and lower concentration of CS led to increased loading efficiency. Finally, particle size is affected by the concentration of the drug, CS, and AuNPs, so that smaller particle sizes can be obtained by increasing the concentration of AuNPs and decreasing the concentration of the drug and CS.

5. Acknowledgment

The authors would like to thank the Faculty of Pharmacy at Isra University for providing funding for this research under grant number 2020/2021/23-5.

6. References

- Bassouini F, ElHalwany N, Abdel Rehim M, Neyfeh M. Advances and new technologies applied in controlled drug delivery system. *Res Chem Intermed*. 2015;41(4):2165-200. <http://dx.doi.org/10.1007/s11164-013-1338-2>.
- Tarafdar J, Sharma S, Raliya R. Nanotechnology: interdisciplinary science of applications. *Afr J Biotechnol*. 2013;12(3):219-26. <http://dx.doi.org/10.5897/AJB12.2481>.
- Wilczewska AZ, Niemirowicz K, Markiewicz KH, Car H. Nanoparticles as drug delivery systems. *Pharmacol Rep*. 2012;64(5):1020-37. [http://dx.doi.org/10.1016/S1734-1140\(12\)70901-5](http://dx.doi.org/10.1016/S1734-1140(12)70901-5).
- Atiyah NA, Albayati TM, Atiya MA. Functionalization of mesoporous MCM-41 for the delivery of curcumin as an anti-inflammatory therapy. *Adv Powder Technol*. 2022;33(2):103417. <http://dx.doi.org/10.1016/j.apt.2021.103417>.
- Alazzawi HF, Salih IK, Albayati TM. Drug delivery of amoxicillin molecule as a suggested treatment for covid-19 implementing functionalized mesoporous SBA-15 with aminopropyl groups. *Drug Deliv*. 2021;28(1):856-64. <http://dx.doi.org/10.1080/10717544.2021.1914778>.
- Ali NS, Alismaeel ZT, Majdi HS, Salih HG, Abdulrahman MA, Cata Saady NM, et al. Modification of SBA-15 mesoporous silica as an active heterogeneous catalyst for the hydroisomerization and hydrocracking of n-heptane. *Heliyon*. 2022;8(6):e09737. <http://dx.doi.org/10.1016/j.heliyon.2022.e09737>.
- Ali NS, Kalash KR, Ahmed AN, Albayati TM. Performance of a solar photocatalysis reactor as pretreatment for wastewater via UV, UV/TiO₂, and UV/H₂O₂ to control membrane fouling. *Sci Rep*. 2022;12(1):16782. <http://dx.doi.org/10.1038/s41598-022-20984-0>.
- Thakkar KN, Mhatre SS, Parikh RY. Biological synthesis of metallic nanoparticles. *Nanomedicine*. 2010;6(2):257-62. <http://dx.doi.org/10.1016/j.nano.2009.07.002>.
- Lee KX, Shameli K, Yew YP, Teow S-Y, Jahangirian H, Rafiee-Moghaddam R, et al. Recent developments in the facile bio-synthesis of gold nanoparticles (AuNPs) and their biomedical applications. *Int J Nanomedicine*. 2020;15:275-300. <http://dx.doi.org/10.2147/IJN.S233789>.
- Khan FA. Synthesis of nanomaterials: methods & technology. In: Khan F, editor. *Applications of nanomaterials in human health*. Singapore: Springer; 2020. p. 15-21. http://dx.doi.org/10.1007/978-981-15-4802-4_2.
- Dong J, Carpinone PL, Pyrgiotakis G, Demokritou P, Moudgil BM. Synthesis of precision gold nanoparticles using Turkevich method. *Kona*. 2020;37(0):224-32. <http://dx.doi.org/10.14356/kona.2020011>.
- Jayeoye TJ, Eze FN, Singh S, Olatunde OO, Benjakul S, Rujiralai T. Synthesis of gold nanoparticles/polyaniline boronic acid/sodium alginate aqueous nanocomposite based on chemical oxidative polymerization for biological applications. *Int J Biol Macromol*. 2021;179:196-205. <http://dx.doi.org/10.1016/j.ijbiomac.2021.02.199>.
- Hutchinson N, Wu Y, Wang Y, Kanungo M, DeBruine A, Kroll E, et al. Green synthesis of gold nanoparticles using upland cress and their biochemical characterization and assessment. *Nanomaterials*. 2021;12(1):28. <http://dx.doi.org/10.3390/nano12010028>.
- Hussain K, Hussain T. Gold nanoparticles: a boon to drug delivery system. *South Indian J. Biol. Sci*. 2015;1(3):127-33.
- Birks JS, Harvey RJ. Donepezil for dementia due to Alzheimer's disease. *Cochrane Database Syst Rev*. 2018;2018(6):CD001190. <http://dx.doi.org/10.1002/14651858.CD001190.pub3>. PMID:29923184.
- Brewster JT 2nd, Dell'Acqua S, Thach DQ, Sessler JL. Classics in chemical neuroscience: donepezil. *ACS Chem Neurosci*. 2019;10(1):155-67. <http://dx.doi.org/10.1021/acscemneuro.8b00517>.
- Baysal I, Ucar G, Gultekinoglu M, Ulubayram K, Yabanoglu-Ciftci S. Donepezil loaded PLGA-b-PEG nanoparticles: their ability to induce destabilization of amyloid fibrils and to cross blood brain barrier in vitro. *J Neural Transm*. 2017;124(1):33-45. <http://dx.doi.org/10.1007/s00702-016-1527-4>.
- Shariatnia Z. Pharmaceutical applications of chitosan. *Adv Colloid Interface Sci*. 2019;263:131-94. <http://dx.doi.org/10.1016/j.cis.2018.11.008>.
- Huang H, Yang X. Synthesis of chitosan-stabilized gold nanoparticles in the absence/presence of tripolyphosphate. *Biomacromolecules*. 2004;5(6):2340-6. <http://dx.doi.org/10.1021/bm0497116>.
- Jhaveri J, Raichura Z, Khan T, Momin M, Omri A. Chitosan nanoparticles-insight into properties, functionalization and applications in drug delivery and theranostics. *Molecules*. 2021;26(2):272. <http://dx.doi.org/10.3390/molecules26020272>.
- Shahidi M, Abazari O, Dayati P, Bakhshi A, Rasti A, Haghirsadat F, et al. Aptamer-functionalized chitosan-coated gold nanoparticle complex as a suitable targeted drug carrier for improved breast cancer treatment. *Nanotechnol Rev*. 2022;11(1):2875-90. <http://dx.doi.org/10.1515/ntrev-2022-0479>.
- Stankus DP, Lohse SE, Hutchison JE, Nason JA. Interactions between natural organic matter and gold nanoparticles stabilized with different organic capping agents. *Environ Sci Technol*. 2011;45(8):3238-44. <http://dx.doi.org/10.1021/es102603p>.
- Amina SJ, Guo B. A review on the synthesis and functionalization of gold nanoparticles as a drug delivery vehicle. *Int J Nanomedicine*. 2020;15:9823-57. <http://dx.doi.org/10.2147/IJN.S279094>.
- Małkiewicz MA, Szarmach A, Sabisz A, Cubała WJ, Szurawska E, Winkiewski PJ. Blood-brain barrier permeability and physical exercise. *J Neuroinflammation*. 2019;16(1):15. <http://dx.doi.org/10.1186/s12974-019-1403-x>.
- Salem DS, Sliem MA, El-Sesy M, Shouman SA, Badr Y. Improved chemo-photothermal therapy of hepatocellular carcinoma using chitosan-coated gold nanoparticles. *J Photochem Photobiol B*. 2018;182:92-9. <http://dx.doi.org/10.1016/j.jphotobiol.2018.03.024>.
- Bujang MA, Sa'at N, Sidik T. Determination of minimum sample size requirement for multiple linear regression and analysis of covariance based on experimental and non-experimental studies. *Epidemiol Biostat Public Health*. 2022;14(3):e12117. <http://dx.doi.org/10.2427/12117>.
- Pereira JM, Muniz JA, Silva CA. Nonlinear models to predict nitrogen mineralization in an Oxisol. *Sci Agric*. 2005;62(4):395-400. <http://dx.doi.org/10.1590/S0103-90162005000400014>.
- Chicco D, Warrens MJ, Jurman G. The coefficient of determination R-squared is more informative than SMAPE, MAE, MAPE,

- MSE and RMSE in regression analysis evaluation. *PeerJ Comput Sci.* 2021;7:e623. <http://dx.doi.org/10.7717/peerj-cs.623>.
29. Bewick V, Cheek L, Ball J. Statistics review 7: correlation and regression. *Crit Care.* 2003;7(6):451. <http://dx.doi.org/10.1186/cc2401>.
 30. Krause A, Dörfler S, Piwko M, Wisser FM, Jaumann T, Ahrens E, et al. High area capacity lithium-sulfur full-cell battery with prelithiated silicon nanowire-carbon anodes for long cycling stability. *Sci Rep.* 2016;6(1):27982. <http://dx.doi.org/10.1038/srep27982>.
 31. Eisa WH, Abdelnaby T, Mostafa S, Elzayat MY. In situ preparation of chitosan/gold nanocomposite: structural and catalytic properties. *Adv Polym Technol.* 2018;37(6):2095-101. <http://dx.doi.org/10.1002/adv.21867>.
 32. Gangane PS, Ghormare NV, Mahapatra DK, Mahajan NM. Gellan gum assisted fabrication and characterization of Donepezil Hydrochloride Mucoadhesive intranasal microspheres. *Int J Curr Res Rev.* 2020;12(19):105-15. <http://dx.doi.org/10.31782/IJCRR.2020.121929>.
 33. Prema P, Thangapandiyam S. In-vitro antibacterial activity of gold nanoparticles capped with polysaccharide stabilizing agents. *Int J Pharm Pharm Sci.* 2013;5:310-4.
 34. Fuster M, Montalbán MG, Carissimi G, Lima B, Feresin GE, Cano M, et al. Antibacterial effect of chitosan-gold nanoparticles and computational modeling of the interaction between chitosan and a lipid bilayer model. *Nanomaterials.* 2020;10(12):2340. <http://dx.doi.org/10.3390/nano10122340>.
 35. Herdiana Y, Wathoni N, Shamsuddin S, Muchtaridi M. Drug release study of the chitosan-based nanoparticles. *Heliyon.* 2022;8(1):e08674. <http://dx.doi.org/10.1016/j.heliyon.2021.e08674>.
 36. Wong PT, Choi SK. Mechanisms of drug release in nanotherapeutic delivery systems. *Chem Rev.* 2015;115(9):3388-432. <http://dx.doi.org/10.1021/cr5004634>.
 37. Atiyah NA, Albayati TM, Atiya MA. Interaction behavior of curcumin encapsulated onto functionalized SBA-15 as an efficient carrier and release in drug delivery. *J Mol Struct.* 2022;1260:132879. <http://dx.doi.org/10.1016/j.molstruc.2022.132879>.
 38. Ali NS, Harharah HN, Salih IK, Cata Saady NM, Zendejboudi S, Albayati TM. Applying MCM-48 mesoporous material, equilibrium, isotherm, and mechanism for the effective adsorption of 4-nitroaniline from wastewater. *Sci Rep.* 2023;13(1):9837. <http://dx.doi.org/10.1038/s41598-023-37090-4>.